JOURNAL OF THERMOPHYSICS AND HEAT TRANSFER
Vol. 23, No. 2, April–June 2009

Rate Parameters for Electronic Excitation of Diatomic Molecules: CN Radiation

Seong-Yoon Hyun,* Chul Park,† and Keun-Shik Chang‡
Korea Advanced Institute of Science and Technology, Daejeon 305-701, Republic of Korea

DOI: 10.2514/1.36749

This is one of an ongoing series of papers on collisional excitation of electronic states in N_2, O_2, NO, CO, CN, and N_2^+. In this paper, CN radiations behind the normal shock wave are calculated using the code SPRADIAN07 for three sets of experimental data taken in shock tubes. For high-pressure conditions, the observed CN radiation is reproduced equally well by the Boltzmann and non-Boltzmann calculations using the SPRADIAN07 code. For intermediate-pressure conditions, the weakly non-Boltzmann radiation is approximately reproduced by the code. For low-pressure, strongly non-Boltzmann, conditions, the existing SPRADIAN07 package fails to reproduce the experimental data. Radiative power loss 6 times that from CN violet and CN red systems must be assumed and the excitation rates must be lowered by 3 orders of magnitude to numerically reproduce the experimental data.

Nomenclature

A_r	=	radiative transition probability, s^{-1}
C	=	constant in k_c, Eq. (7)
c	=	continuum (free) state
D_a	=	activation energy in k_c, Eq. (7), eV
H	=	total enthalpy, J/kg
I_λ	=	specific intensity, $W/(cm^2 \cdot \mu s \cdot sr)$
i, j	=	bound electronic states of molecule
K_e	=	rate coefficient of excitation by electron collision, cm^3/s
K_{eq}	=	equilibrium constant
K_h	=	rate coefficient of excitation by heavy-particle collision, cm^3/s
K'_h	=	modified rate coefficient of excitation by heavy-particle collision, Eqs. (6) and (7), cm^3/s
k	=	total number of electronic states
k_B	=	Boltzmann constant, J/K
k_c	=	correction factor to $K_h(1, 2)$, Eq. (7)
k_λ	=	absorption coefficient, cm^{-1}
n_i	=	number density of state i, cm^{-3}
$n_{i,eq}$	=	hypothetical equilibrium number density of electronic state i, cm^{-3}
n_m	=	nonequilibrium number density of molecule, cm^{-3}
$n_{m,eq}$	=	hypothetical equilibrium number density of molecule, cm^{-3}
p	=	pressure, torr
Q_r	=	radiative power loss of CN violet and CN red, $J/(kg \cdot s)$
Q'_r	=	$\zeta \times Q_r$, Eq. (12), $J/(kg \cdot s)$
s	=	an exponent in diffusion correction for vibrational relaxation time, Eq. (2)
s	=	distance along a ray, cm
T	=	heavy-particle translational–rotational temperature, K
T_{av}	=	geometric average temperature, K ($\sqrt{T_v T}$)
T_d	=	activation temperature, K
T_{sh}	=	heavy-particle translational–rotational temperature immediately behind the shock, K
T_v	=	vibrational-electron-electronic (vibroelectronic) temperature, K
$T_{v,sh}$	=	vibroelectronic temperature immediately behind the shock, K
t	=	time, s
U_{sh}	=	shock velocity, km/s
x	=	distance from shock front, cm
α	=	absorption power, W/cm^3
γ	=	specific heat ratio
ε	=	emission power, W/cm^3
ϵ_v	=	vibroelectronic energy, J/kg
$\epsilon_{v,eq}$	=	vibroelectronic energy under equilibrium, J/kg
ε_λ	=	emission coefficient, $W/(cm^3 \cdot \mu m \cdot sr)$
η_i	=	ratio of nonequilibrium to equilibrium population of state i ($n_i/n_{i,eq}$)
κ_i	=	nonequilibrium factor of state i (η_i/χ)
ρ	=	density, kg/cm^3
ρ_{sh}	=	density immediately behind the shock, kg/cm^3
τ_v	=	vibrational relaxation time, s
χ	=	ratio of nonequilibrium to equilibrium species density ($n_m/n_{m,eq}$)

Subscripts

e	=	electron
eq	=	equilibrium
h	=	heavy particle
i, j	=	bound electronic states of molecule
m	=	molecule
∞	=	freestream

Presented as Paper 1276 at the 46th AIAA Aerospace Sciences Meeting and Exhibit, Reno, NV, 7–10 January 2008; received 20 January 2008; revision received 3 September 2008; accepted for publication 3 September 2008.

*Graduate Student, Department of Aerospace Engineering; heinne@kaist.ac.kr. Student Member AIAA.
†Professor, Department of Aerospace Engineering. Fellow AIAA.
‡Professor, Department of Aerospace Engineering. Member AIAA.

I. Introduction

RADIATON under a non-Boltzmann distribution of internal states could be substantially different from that of Boltzmann distribution in some cases of planetary entry flights. In such cases, the non-Boltzmann effects will have to be accounted for to better design the required heat shields. There exist several radiation codes (e.g., NEQAIR85 [1], NEQAIR96 [2], SPRADIAN [3], and PARADE [4]). In most of these codes, attempts have been made to compute the non-Boltzmann effects. The basic schemes for calculating non-Boltzmann effects are well known [5]: the internal states are assumed to be distributed according to the so-called quasi-steady-state (QSS) conditions. The QSS distribution is dictated by the rates by which the transitions occur among bound states or between the bound states

and free state. These rate constants for state-to-state transitions must be supplied by the user.

For the atomic systems, the needed rate-coefficient data are given in the original NEQAIR [1] and are shared by all other existing such codes. However, for the calculation of the non-Boltzmann effects in diatomic systems, the data base has hitherto been incomplete. In the existing codes, only the electron-impact phenomena have been accounted for in calculating state-to-state transitions. Even for these, the data set is that based on information available before 1990. The state-to-state transitions due to collisions of heavy particles are not accounted for in the existing code packages.

A new radiation package called SPRADIAN07 (Structured Package for Radiation Analysis 2007) has been developed jointly by the Korea Advanced Institute of Science and Technology (KAIST) and Japan Aerospace Exploration Agency (JAXA) to address these issues. A new set of rates of state-to-state transitions by electron impact has been constructed in [6] from the most up-to-date information. The state-to-state transitions due to collisions of heavy particles are accounted for, and the needed rate coefficients are also derived from the up-to-date information [7]. Though not related directly to the non-Boltzmann issue, the code also accurately accounts for various symmetries in the diatomic system.

This is one of an ongoing series of papers on collisional excitation of electronic states in N_2, O_2, NO, CO, CN, and N_2^+. The purpose of the present study is to verify the accuracy of the SPRADIAN07 and the input data through computations of CN radiation under both Boltzmann and supposedly non-Boltzmann excitations. CN is an important radiator in air and in Mars, Venus, and Titan entries. The calculations are carried out for the CN violet, $B^2\Sigma^+$–$X^2\Sigma^+$, and CN red, $A^2\Pi$–$X^2\Sigma^+$, bands to compare with the three experimental measurements: 1) CN violet radiation in Mars entry conditions obtained by the KAIST group [8], 2) CN violet and CN red radiation in Titan entry conditions by the Marseille University group [9], and 3) CN violet and CN red radiations in Titan entry conditions obtained by the NASA Ames Research Center group [10].

For the KAIST data, which was obtained at relatively high pressures, the present work finds that the radiation intensities of the CN violet calculated under the non-Boltzmann assumption is almost the same as that calculated assuming the Boltzmann distribution, and the SPRADIAN07 code numerically reproduces those accurately. For the Marseille University data, which was taken in an intermediate-pressure range and produces weakly non-Boltzmann distributions, the profiles of the CN radiations are at least partly approximately reproduced by the SPRADIAN07 code. For the NASA Ames data, which was obtained at very low pressures and produces strongly non-Boltzmann distributions, the observed experimental data can be almost reproduced by assuming a large radiative power loss and heavy-particle-impact excitation rates 3 orders of magnitude smaller than the values in the SPRADIAN07 package.

II. Numerical Simulation

A. Flowfield Calculation

A one-dimensional space-marching calculation is performed to determine the properties of the nonequilibrium reacting flows behind a normal shock wave produced in a shock tube. The initial conditions are calculated by the normal shock relations using the specific heat ratio ; the known experimental conditions of p_∞, T_∞, and $T_{v,\infty}$; the measured $U_{\rm sh}$; and the species chemical composition. The initial value of the vibroelectronic temperature $T_{v,\infty}$ is taken to be 3000 K to account for the shock-slip phenomenon [11].

To calculate equilibrium constants for chemical reactions containing polyatomic molecules, both partition function and JANNAF methods are employed: the partition function method is used for the small molecules such as atoms, diatoms, and triatoms, and the JANNAF method is used for the large polyatomic molecules. The equilibrium constants are evaluated at five temperatures, 5000, 6750, 8500, 10,250, and 12,000 K. The calculated values are fitted by an expression of the form

$$K_{\rm eq}(T) = \exp[a_1/z + a_2 + a_3 \ln z + a_4 z + a_5 z^2] \tag{1}$$

where $z = 10,000/T$.

Chemical reactions are computed using the two-temperature model proposed by Park [12]. All dissociation reactions by heavy-particle impact are controlled by $T_{\rm av}$, all electron-impact dissociation and ionization reactions are governed by T_v, and the reactions of all exchange and associative ionization are governed by T. We assume that heavy-particle translational and rotational temperatures equilibrate immediately behind the shock wave.

To account for the translational–vibrational energy exchange, the Landau–Teller model [5,13] and the bridging [5,14] model are used. The bridging model is given by

$$\frac{\partial \epsilon_v}{\partial t} = \frac{\epsilon_{v,\rm eq}(T) - \epsilon_v(T_v)}{\tau_v} \left| \frac{T_{\rm sh} - T_v}{T_{\rm sh} - T_{v,\rm sh}} \right|^{s-1} \tag{2}$$

where $s = 3.5\exp(-5000/T_{\rm sh})$, time τ_v is the sum of the Landau–Teller relaxation time calculated by the expression of Millikan and White [15] and the collision-limited relaxation time [5,12]. Equation (2) describes the Landau–Teller model when $s = 1$.

We also take into account the preferential dissociation phenomenon in determining the rate of change of vibrational energy [5]: the vibrational energy is increased or decreased by 30% of the dissociation energy [16]. For the change of electron-electronic energy, three terms are considered [5]: electron-impact dissociation, electron-impact ionization, and elastic energy transfer between electrons and heavy particles. The loss or gain of electron energy is 80% for both dissociation and ionization energies in electron-impact dissociation and ionization.

B. Radiation Calculation

The code SPRADIAN07 solves the radiative transfer equation $\mathrm{d}I_\lambda/\mathrm{d}s = \varepsilon_\lambda - k_\lambda I_\lambda$ along a line of sight by assuming that emission and absorption coefficients vary linearly between two given points. The emission and absorption coefficients ε_λ and k_λ are computed using the line-by-line technique in this code. Electronic–vibrational transition moments are taken from the work of Laux [17] for CN violet and from Bauschlicher et al. [18] for CN red. The Hönl–London factors for $^2\Sigma$–$^2\Sigma$ and $^2\Pi$–$^2\Sigma$ transitions are formulated from the book by Kovács [19] and divided by a factor of 2, accounting for spin degeneracy [20].

1. *Quasi-Steady-State Master Equation*

As mentioned, the SPRADIAN07 computes both Boltzmann and non-Boltzmann radiations from temperatures and species number densities at each point in the flow. Under non-Boltzmann excitation, the QSS master equation [5] is solved. The master equation for the population of the electronic energy states is, in general, written as

$$\begin{aligned}\frac{\partial n_i}{\partial t} &= \sum_{j=1}^{k}[K_h(j,i)n_h + K_e(j,i)n_e]n_j \\ &\quad + [K_h(c,i)n_h + K_e(c,i)n_e]n_1 n_2 + \sum_{j=1}^{k} A_r(j,i)n_j \\ &\quad - \sum_{j=1}^{k}[K_h(i,j)n_h + K_e(i,j)n_e]n_i \\ &\quad - [K_h(i,c)n_h + K_e(i,c)n_e]n_i - \sum_{j=1}^{k} A_r(i,j)n_i\end{aligned} \tag{3}$$

where $K_h(j,i)$, for example, represents the rate coefficient for the transition from the electronic states j to i by heavy-particle impact. The QSS condition exists when the variation of n_i over time is negligibly small compared with the incoming and outgoing rates. The QSS condition is imposed by setting the left-hand side of Eq. (3) to zero. Three nonequilibrium parameters are defined: the normalized population of state i (η_i) is defined as the ratio of the

Table 1 Bound–bound electronic excitation-rate coefficient of CN by heavy-particle impact in an Arrhenius form: $K_h(i,j) = A(T/6000)^n \exp(-T_d/T)$ and cm^3/s

	1–2, $X^2\Sigma^+$–$A^2\Pi$			2–3, $A^2\Pi$–$B^2\Sigma^+$			3–4, $B^2\Sigma^+$–$a^4\Sigma^+$			4–5, $a^4\Sigma^+$–$D^2\Pi$		
M[a]	A[b]	n	T_d	A	n	T_d	A	n	T_d	A	n	T_d
N	8.26^{-09}	0.047	18,988	1.21^{-09}	0.041	29,098	3.75^{-09}	0.508	10,249	3.83^{-10}	0.50	31,774
O	7.71^{-09}	0.062	17,794	1.13^{-09}	0.057	28,904	3.75^{-09}	0.508	10,249	3.83^{-10}	0.50	31,774
N_2	1.95^{-07}	−1.899	42,648	6.66^{-10}	0.271	26,301	1.65^{-15}	0.508	10,249	1.69^{-16}	0.50	31,774
O_2	5.67^{-09}	0.132	17,943	6.33^{-10}	0.283	26,159	3.75^{-09}	0.508	10,249	3.83^{-10}	0.50	31,774
NO	5.81^{-09}	0.127	18,010	8.49^{-10}	0.122	28,121	3.75^{-09}	0.508	10,249	3.83^{-10}	0.50	31,774
CO	1.92^{-08}	−0.555	26,310	2.80^{-09}	−0.561	36,420	6.26^{-10}	0.508	10,249	6.40^{-11}	0.50	31,774

[a]Colliding heavy particle.
[b]A in cm^3/s and $0.00^{-00} \equiv 0.00 \times 10^{-00}$.

calculated nonequilibrium population n_i to the hypothetical equilibrium population $n_{i,\mathrm{eq}}$; the normalized molecule density χ is defined as the ratio of the given nonequilibrium species density under consideration, n_m, to the hypothetical equilibrium species density

$$n_{m,\mathrm{eq}}\left(=\sum_1^k n_{i,\mathrm{eq}}\right)$$

and the ratio of η_i to χ is defined as κ_i. When the detailed balances are applied, Eq. (3) becomes

$$\begin{aligned} &K_e(i,c)\frac{n_{i,\mathrm{eq},e}}{n_{i,\mathrm{eq},h}}\frac{n_e}{n_h} + K_h(i,c) \\ &= -\sum_{j=1}\left[K_e(i,j)\frac{n_{i,\mathrm{eq},e}}{n_{j,\mathrm{eq},e}}\frac{n_{j,\mathrm{eq},h}}{n_{i,\mathrm{eq},h}}\frac{n_e}{n_h} + K_h(i,j)\right. \\ &\left. + \frac{A_r(j,i)}{n_h}\frac{n_{j,\mathrm{eq},h}}{n_{i,\mathrm{eq},h}}\right]\eta_j + \left\{K_e(i,c)\frac{n_e}{n_h} + K_h(i,c)\right. \\ &\left. + \sum_j\left[K_e(i,j)\frac{n_e}{n_h} + K_h(i,j) + \frac{A_r(i,j)}{n_h}\right]\right\}\eta_i \end{aligned} \tag{4}$$

This forms k linear algebraic equations for vector η_j, and can be expressed in a matrix form as

$$\mathbf{M}(i,j)\eta = \mathbf{C}(i) + \mathbf{D}(i)\chi, \qquad \eta = [\mathbf{M}]^{-1}\mathbf{C} + [\mathbf{M}]^{-1}\mathbf{D}\chi \tag{5}$$

where $\mathbf{M}$ is a matrix, and $\mathbf{C}$ and $\mathbf{D}$ are vectors. When $i = 1$,

$$M(1,j) = n_{j,\mathrm{eq}}\Big/\sum_1^k n_{i,\mathrm{eq}}$$

$C(1) = 0$, and $D(1) = 1$. When $i \neq 1$, the diagonal and offdiagonal elements of $\mathbf{M}$ are expressed according to the right-hand side of Eq. (4), and the vectors of $C(i)$ and $D(i)$ are equal to the left-hand side of Eq. (4) and 0, respectively.

2. Excitation-Rate Coefficient

For the CN molecule, five electronic states ($X^2\Sigma^+$, $A^2\Pi$, $B^2\Sigma^+$, $a^2\Sigma^+$, and $D^2\Pi$) are considered in the SPRADIAN07 package. The dissociation energy of the ground state, D_0, is 61,631 cm^{-1}. The SPRADIAN07 calculates the $K_e(i,j)$ using electron-impact excitation cross sections that are tabulated in [6]. The basic formulation is described in [5]. The $K_e(i,c)$ are also tabulated in [6]. The values of $K_h(i,j)$ are deduced in [7] from the experimental quenching rates. The $K_h(i,c)$ are also estimated in [7] from the known rate coefficients for dissociation from the ground electronic state. The colliding heavy particles considered are N, O, N_2, O_2, NO, and CO. In Table 1, the parameters in the $K_h(i,j)$ values used are listed.

In addition to the K_h given in Table 1, an arbitrarily modified set of K_h, named K'_h, is considered for the CN molecule

$$K'_h(i,j) = K_h(i,j)/3 \tag{6}$$

for all transitions except the $X^2\Sigma^+ - A^2\Pi$ transition:

$$K'_h(1,2) = k_c \times K_h(1,2) \quad \text{with } k_c = C \times \exp\left(-\frac{D_a}{k_B T}\right) \tag{7}$$

where the parameters C and D_a are chosen depending on the flow conditions. This K'_h is introduced because it can numerically reproduce all three experimental data set better than K_h, though the reason is unknown. The K'_h values so calculated and the implied cross sections are shown in Fig. 1 for the conditions of Titan entry case b, described in the next section. Its conditions are the 5%CH_4–95%N_2 mixture, the shock speed $U_{\mathrm{sh}} = 5.56$ km/s, and the freestream pressure $p_\infty = 0.1$ torr. As seen here, the cross sections implied by K'_h are reasonable.

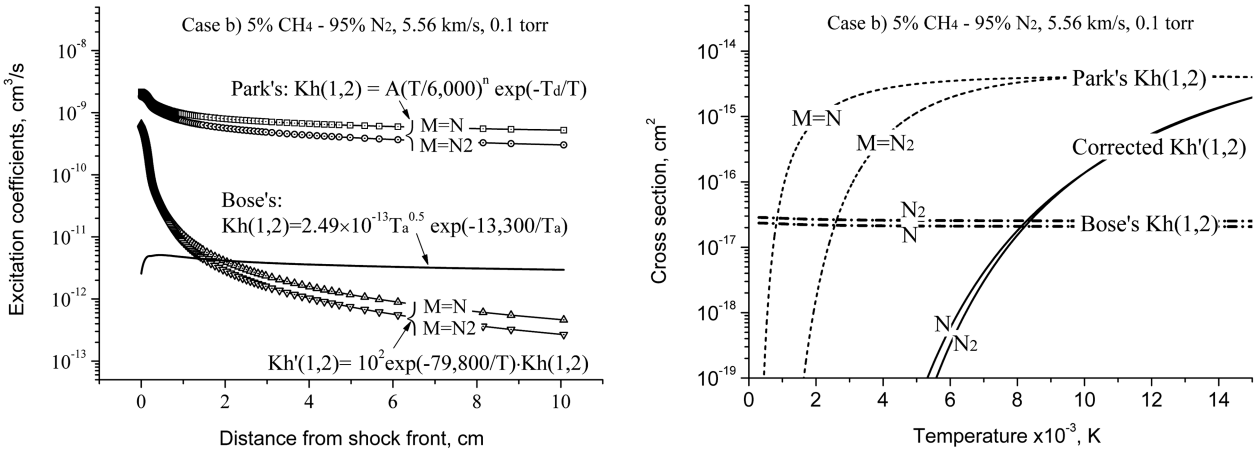

a) Excitation coefficients **b) Cross sections**

Fig. 1 Comparisons of the modified excitation coefficients for the $X^2\Sigma^+$–$A^2\Pi$ transition and their implied cross sections with those of Park [7] and Bose et al. [10].

3. Validity of the QSS Assumption

Validity of the QSS assumption was tested first by Levin et al. [21,22], who reported that the QSS approximation agreed with an exact solution in their analysis of electronic population of a NO molecule. In the present work, a simpler test was made. To verify the validity of the QSS assumption, the sum of incoming rates and the sum of outgoing rates are compared with $\partial n_i/\partial t$ for the conditions of Titan entry case b, mentioned previously. We introduce Δt as a time scale of change of conditions [23]:

$$\frac{1}{n_i}\frac{\partial n_i}{\partial t} = \frac{1}{\Delta t_i} \tag{8}$$

For the CN $A^2\Pi$ state ($i = 2$), the dominant term of incoming rates in Eqs. (3) and (4) is the term expressing excitation from the ground state; that is,

$$K_h(2,1)\frac{n_{2,\mathrm{eq},h}}{n_{1,\mathrm{eq},h}}\frac{n_1}{n_2}n_h$$

For the CN $B^2\Sigma^+$ state ($i = 3$), the dominant term is the excitation from the $A^2\Pi$ state; that is,

$$K_h(3,2)\frac{n_{3,\mathrm{eq},h}}{n_{2,\mathrm{eq},h}}\frac{n_2}{n_3}n_h$$

To satisfy the QSS condition, these leading terms should be much greater than Δt_2^{-1} and Δt_3^{-1}, respectively:

$$\Delta t_2 \gg \frac{1}{K_h(2,1)}\frac{n_{1,\mathrm{eq},h}}{n_{2,\mathrm{eq},h}}\frac{n_2}{n_1}\frac{1}{n_h}, \qquad \Delta t_3 \gg \frac{1}{K_h(3,2)}\frac{n_{2,\mathrm{eq},h}}{n_{3,\mathrm{eq},h}}\frac{n_3}{n_2}\frac{1}{n_h} \tag{9}$$

For the condition of consideration, the left-hand sides are found to be 2 orders of magnitude larger than the right-hand sides.

4. Radiative Power Loss

Emission and self-absorption powers ε and α are calculated as

$$\varepsilon = \int_\Omega\int_\lambda \varepsilon_\lambda \mathrm{d}\lambda\mathrm{d}\Omega, \qquad \alpha = \int_\Omega\int_\lambda k_\lambda I_\lambda \mathrm{d}\lambda\mathrm{d}\Omega \tag{10}$$

The change of radiative power loss at each time is defined as

$$Q_r = -\frac{(\varepsilon-\alpha)_{\mathrm{CN\ violet,red}} + (\varepsilon-\alpha)_{\mathrm{CO4+}}}{\rho} \tag{11}$$

In evaluating I_λ in Eq. (10), radiative transfer equation is integrated along the optical axis. The diameter of the shock tube is the path length. Questions may be raised as to whether the wall of the shock-tube reflected radiation, so that the effective path length of radiation along the optical axis is longer than the shock-tube diameter. Such concern is unnecessary because in all shock-tube experiments considered here, both sides of the shock-tube wall in the test section consisted of transparent windows.

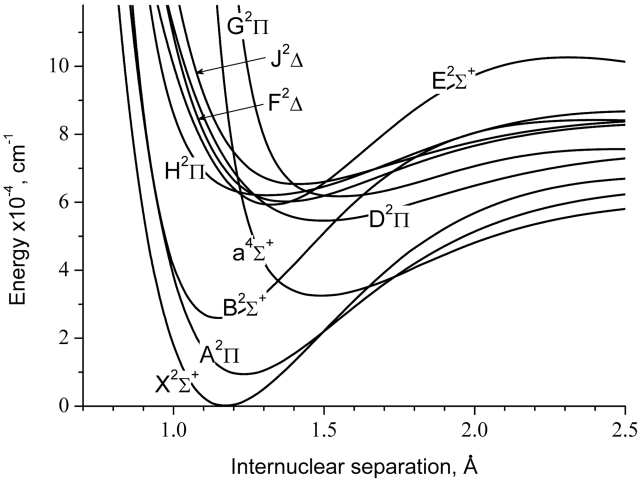

Fig. 2 Molecular interaction potentials of electronic states of CN molecule.

It is generally believed that the strongest radiation in the environments of present concern emanate from the CN violet and CN red systems. Hence, the ε and α in Eq. (10) and resulting Q_r can be calculated accounting only for these two band systems. In the present work, such Q_r is considered first. Next, attention is given to the fact that there are many other radiating mechanisms in CN in the vacuum-ultraviolet (VUV)-wavelength range. The potential diagram of the CN molecule is not available for some highly excited states in literature. We constructed the CN potentials by using the known molecular constants [24–27], as shown in Fig. 2. Their dissociation limits were estimated from the book by Herzberg [28]. As shown, $E^2\Sigma^+$, $F^2\Delta$, $G^2\Pi$, $H^2\Pi$, and $J^2\Delta$ are known, in addition to the previously mentioned five states.

Douglas and Routly [25] found and analyzed four band systems of CN: $H^2\Pi$–$B^2\Sigma^+$, $F^2\Delta$–$A^2\Pi$, $D^2\Delta$–$A^2\Pi$, and $D^2\Delta$–$X^2\Sigma^+$ in the 200–300 nm wavelength range. They additionally mentioned the possibility of stronger VUV radiations from some unknown bands (e.g., $H^2\Pi$–$X^2\Sigma^+$). Lutz [26] also reported $F^2\Delta$–$A^2\Pi$ and $E^2\Sigma^+$–$A^2\Pi$ bands at 200–250 nm. Huber et al. [29] observed the $L^2\Sigma$–$A^2\Pi$ band in the Schumann region. Schaefer and Heil [27] and Lavendy et al. [30] theoretically studied electronic states of CN and showed that there are many electronic states, some of which are experimentally known and some of which are unknown. Many $^2\Sigma$ and $^2\Pi$ states were reported by Lavendy et al. [30], and calculated transition moments of the $^2\Sigma^+$–$X^2\Sigma^+$ and $^2\Pi$–$X^2\Sigma^+$ transitions were found to be much larger than those of the $B^2\Sigma^+$–$X^2\Sigma^+$ transition. Based on these, one expects that there are many strong radiative transitions in the VUV-wavelength range that terminate at

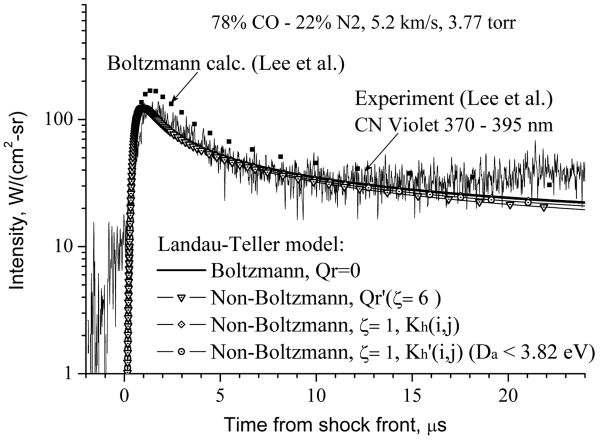

a) Landau-Teller model

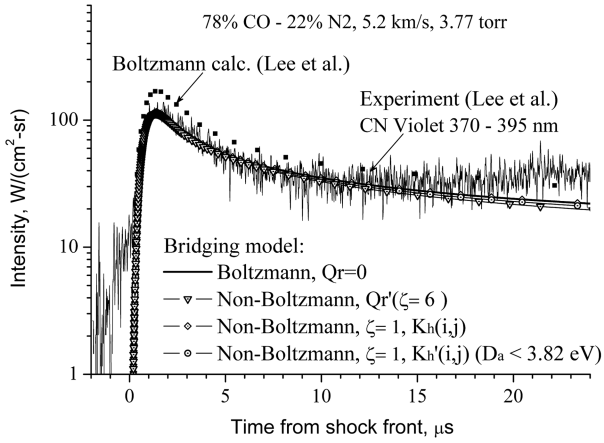

b) Bridging model

Fig. 3 Intensity profiles of CN violet with the Landau–Teller and bridging models for the Mars entry condition of Lee et al. [8].

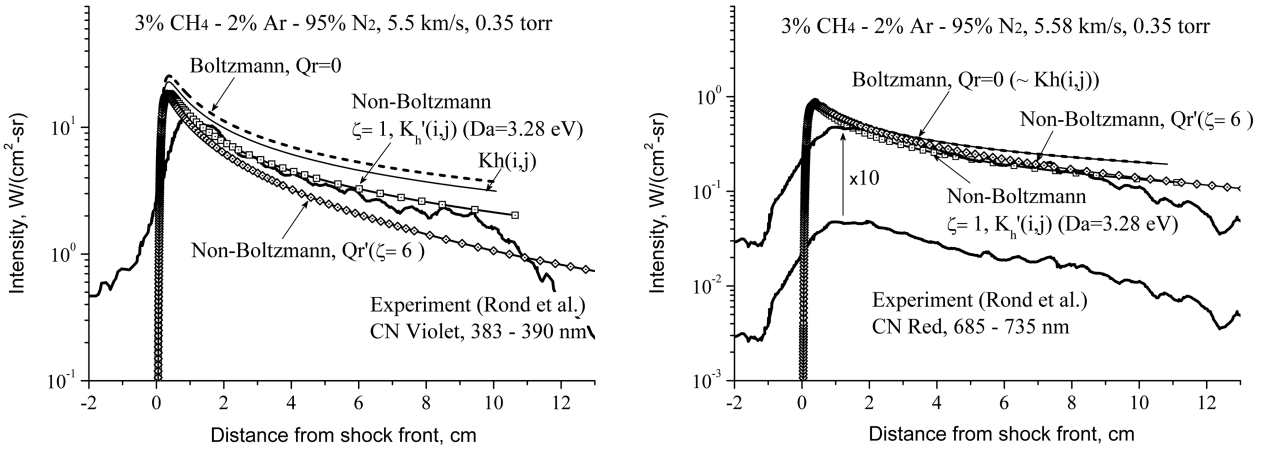

a) CN violet **b) CN red**

Fig. 4 Intensity profiles of CN violet and CN red with the Landau–Teller model for the Titan entry conditions of Rond et al. [9].

the $X^2\Sigma^+$, $A^2\Pi$, or $B^2\Sigma^+$ state. These bands produce not only line radiation as bands, but continuum radiation via several complicated processes. Line radiation tends to be partly self-absorbed, but the continuum radiation is nearly optically thin in the environment of shock-tube experiments. This means that the radiative power loss is most likely much greater than that calculated by accounting only for the violet and red systems. For this reason, a modified radiative power loss Q'_r, which is $\zeta \times Q_r$,

$$Q'_r = \zeta \times Q_r \text{ (CN violet and CN red only)} \qquad (12)$$

is considered. As will be shown later, the ζ value of 6 fits the existing experimental data best.

III. Comparisons with Experiments

A. Mars Conditions by the KAIST Group

Lee et al. [8] of KAIST studied the radiation of the CN violet band in a shock-tube flow simulating Mars entry conditions. They obtained the calibrated absolute intensities from a 78%CO–22%N_2 mixture behind a reflected-shock wave. The initial gas pressures in the test section were from 3.77 to 8.37 torr with the equivalent shock velocities of 4.8 to 5.2 km/s. The diameter of the shock tube was 4.75 cm. The reflected-shock pressure was between 1.36 and 2.99 atm. They analyzed their experimental data using the NEQAIR85 [1] code. Their intensity profiles calculated under the

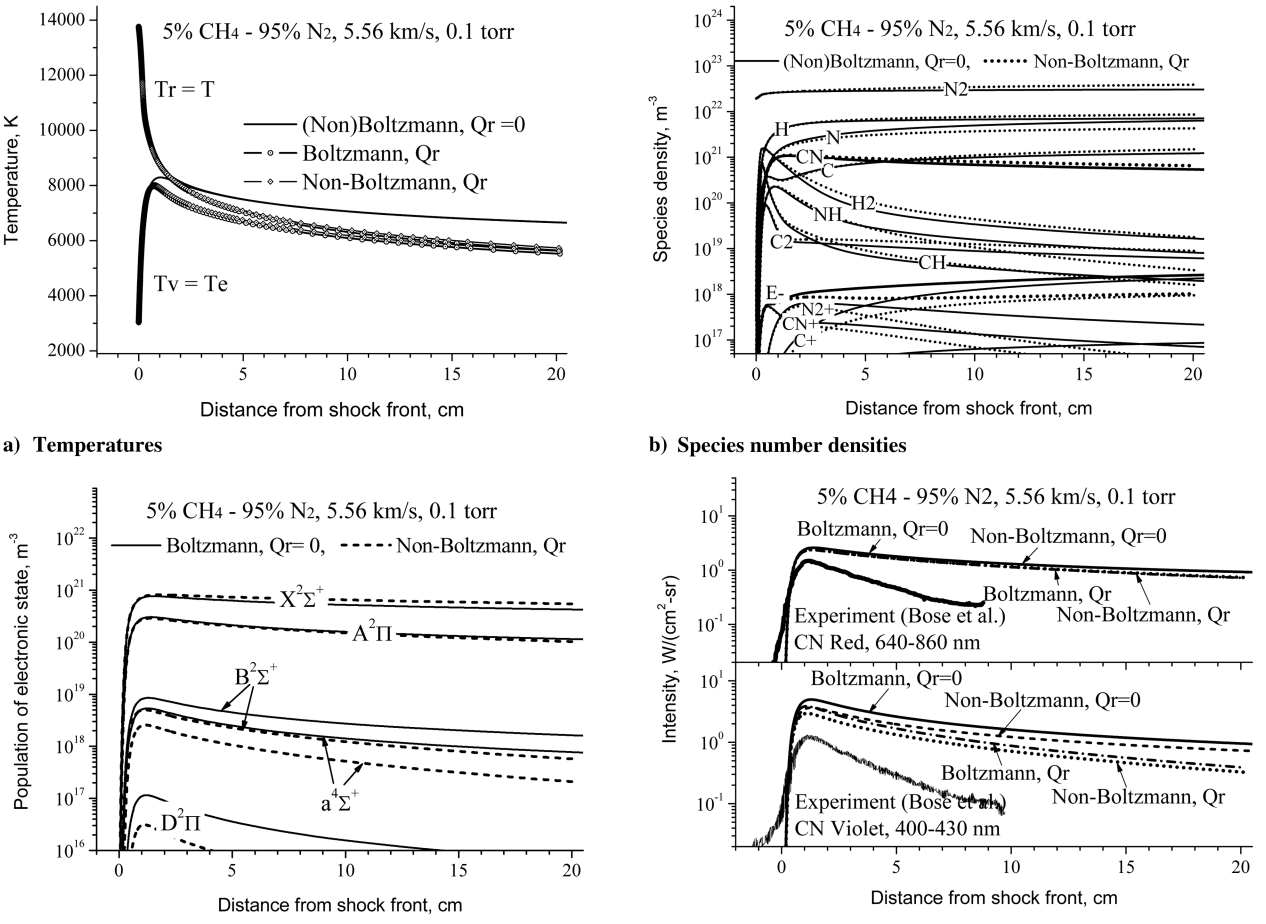

a) Temperatures **b) Species number densities**

c) Populations of electronic states of CN molecule **d) Intensities of CN red and CN violet**

Fig. 5 Profiles of calculated flowfield and radiation for case b of Bose et al [10] data with Q_r and K_h.

Boltzmann excitation assumption overpredicted the measurements by up to 40%, depending on the experimental conditions.

Calculations were performed in the present work using the SPRADIAN07 code for the conditions of shock velocity $U_{sh} = 5.2$ km/s and freestream pressure of $p_\infty = 3.77$ torr. Both Landau–Teller and bridging models were used. The Boltzmann and non-Boltzmann radiations were carried out for the Park–Lesov–Gökçen–Tsang chemical-reaction model [8]. N, O, N_2, O_2, NO, CO, and electrons were considered as colliders in the non-Boltzmann calculation. The wavelength region was from 370 to 395 nm. The radiative power loss by the CO fourth positive system in the VUV-wavelength range was taken into account in determining the radiative power losses Q_r and Q'_r.

The present results are presented in Fig. 3. The figure shows the results of calculations: Boltzmann radiation without the radiative power loss ($\zeta = 0$), non-Boltzmann radiation with Q'_r ($\zeta = 6$), and non-Boltzmann radiation with K_h and K'_h. As seen in the figure, all calculations (i.e., Boltzmann or non-Boltzmann with Q_r or Q'_r or with K_h or K'_h) agree with the experimental data within the scatter of experimental data to the flow time of up to 12 μs. The nonequilibrium factor κ was found to be between 0.98 and unity for the CN $A^2\Pi$, $B^2\Sigma^+$, and $a^2\Sigma^+$ states. That is, the distribution of the internal states was nearly Boltzmann. Note here also that the slope of the rise to the peak intensity is well reproduced. This implies that the spatial resolution was high in the experiment. Such high spatial resolution can be obtained by making the solid angle of acceptance small. A small solid angle was allowed in this experiment because pressure was high. Such good agreement in all aspects of this experiment is believed to be a result of the high pressure in this experiment.

The deviation between the experiment and the calculation after 12 μs can be attributed to the onset of boundary-layer growth on the shock-tube wall: boundary-layer growth has an effect of compressing the test gas. The agreement seen here up to 12 μs verifies the accuracy of the method of calculation used here (i.e., the method of flow condition calculation, the SPRADIAN07 code, and the intensity parameters for the CN violet under the Boltzmann condition).

B. Titan Conditions by the Marseille University Group

Rond et al. [9] of Marseille University carried out a shock-tube experiment to determine the radiation intensity of CN violet and CN red during Titan entry. The measurement was made behind the primary shock wave. Calculation was made in the present work for two cases: a) CN violet at $U_{sh} = 5.5$ km/s and $p_\infty = 0.35$ torr and b) CN red at $U_{sh} = 5.58$ km/s and $p_\infty = 0.35$ torr. Initial species concentrations are the same for both cases: 3%CH_4–2%Ar–95%N_2 by volume. The Landau–Teller and bridging models with the reduced-chemical-reaction set of Gökçen [31] were employed. N, N_2, and electrons were taken into account as colliders in the QSS computation. The lateral depth was 7.0 cm, and the wavelengths covered from 383 to 390 nm for CN violet and from 685 to 735 nm for CN red. Rond et al. [9] presented their experimental data against laboratory time. Their time scale was converted to distance in centimeters in the present work. The conversion relation is

$$x = \frac{\rho_\infty}{\rho_{sh}} \times U_{sh} \times \text{particle time}$$

This relationship was approximated in the present work by the assumption that the particle time is 6 times larger than the laboratory

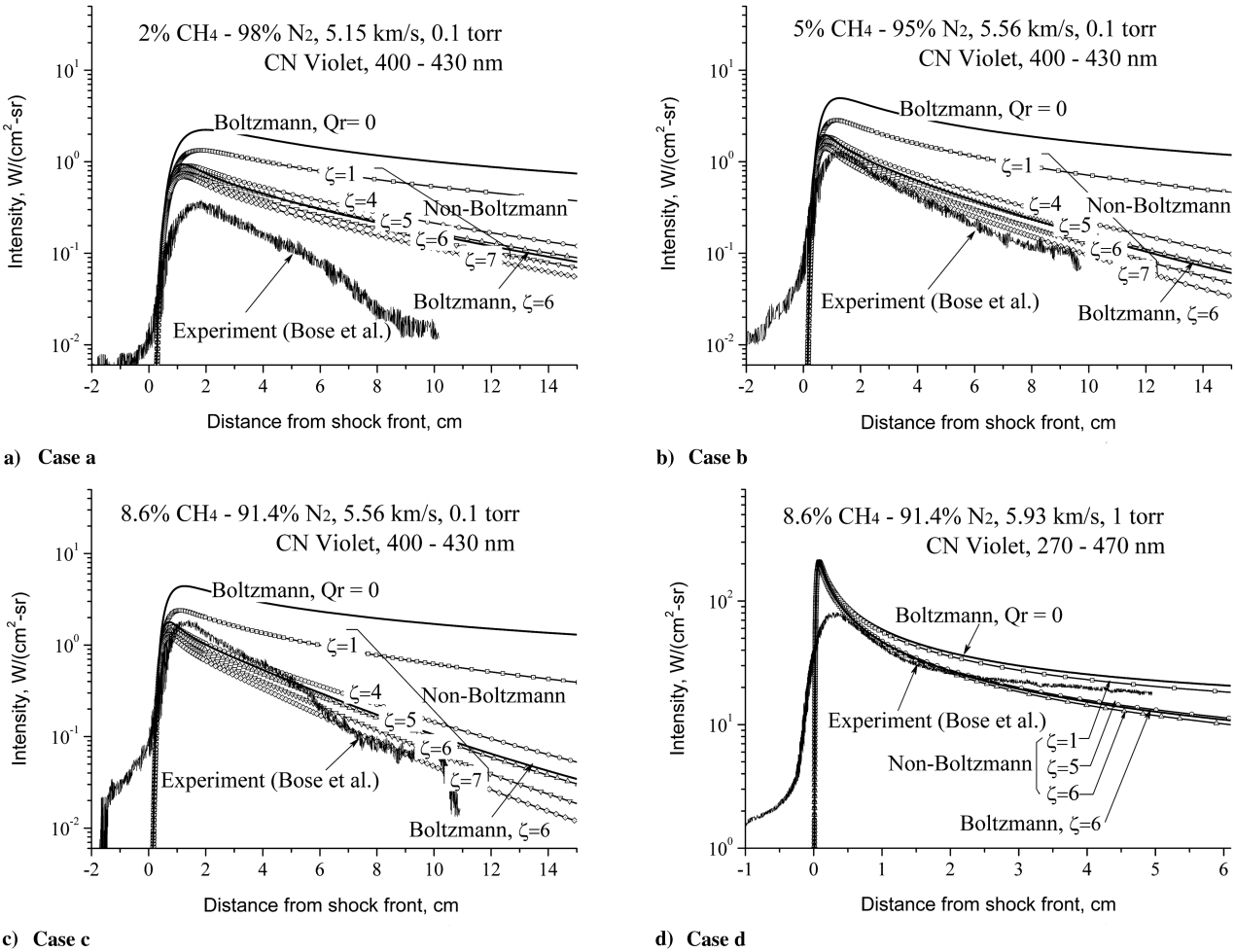

Fig. 6 Radiation profiles of CN violet for cases a–d of Bose et al. [10] with the Landau–Teller model and with Q'_r and K_h.

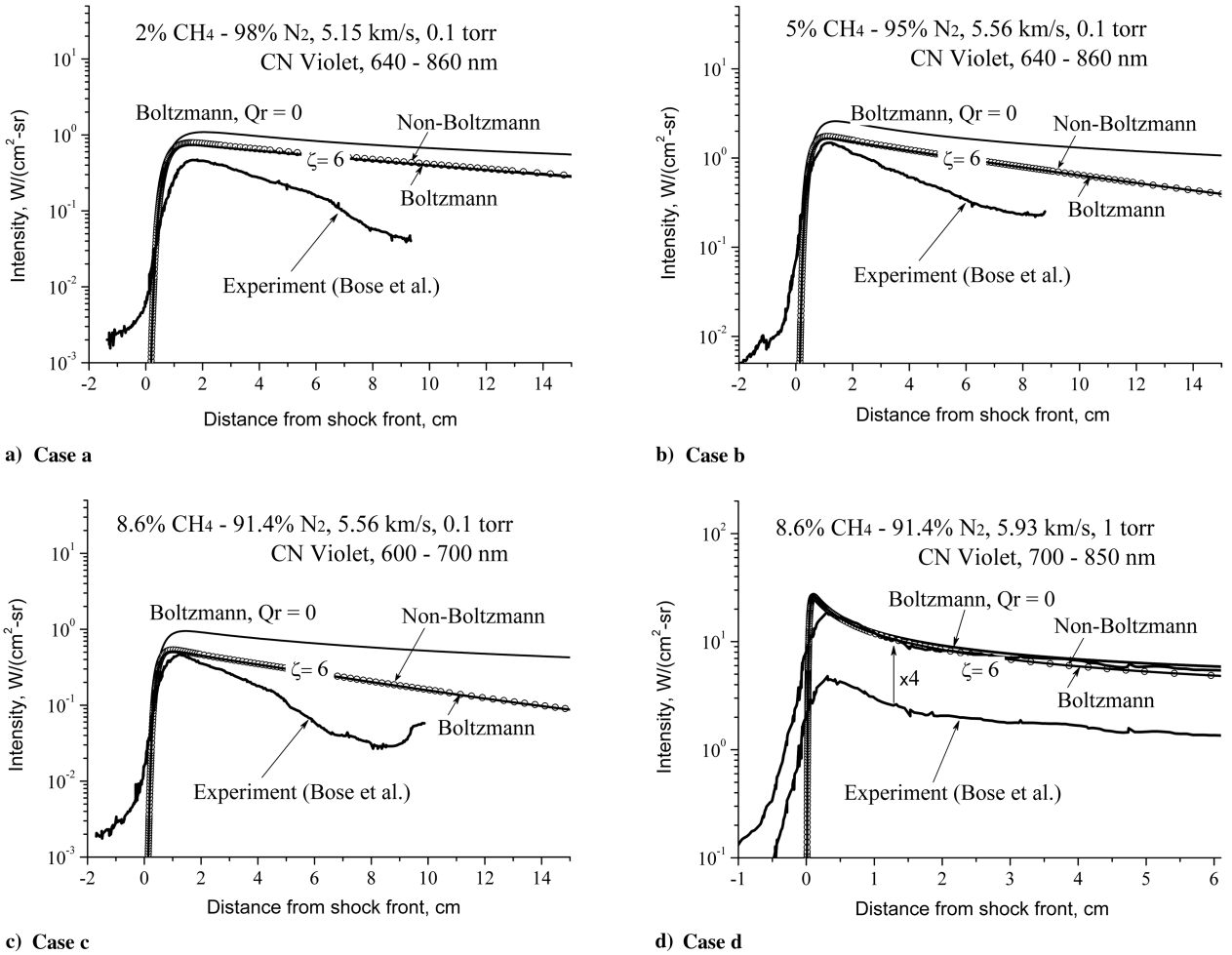

Fig. 7 Radiation profiles of CN red for cases a–d of Bose et al. [10] with the Landau–Teller model and with Q'_r and K_h.

time. When calculating K'_h, then k_c in Eq. (7) is taken to be $k_c = 1.0 \times \exp(-38,100/T)$.

Because these experiments are conducted at a pressure lower than those made by Lee et al. [8], one expects to see non-Boltzmann effects. But the pressure was still higher than that for the NASA Ames experiment mentioned in the next section. For this reason, the pressures in this experiment can be considered to be intermediate pressures. The results of the present calculations for non-Boltzmann excitation are shown in Fig. 4. All of the present calculations made using different methods give decay rates of both CN violet and CN red that are not much different from the experimental values. The intensity decay rate of CN violet is slightly faster when Q'_r ($\zeta = 6$) is used. However, for CN red, Q'_r ($\zeta = 6$) and K'_h with Q_r ($\zeta = 1$) give almost the same intensity values.

As the figure shows, the initial rise to the peak in experiment is much slower than in the calculation, unlike for the KAIST data. This is a sign of spatial smearing; because either the solid angle of acceptance was large or the beam was out of focus, the radiation over about a 2 cm volume was averaged in the experiment. Presumably, the solid angle of acceptance had to be large because radiation was weak. Note that this has little influence on the absolute intensity or the slope of its decay after the peak radiation point. Otherwise, the calculated CN red intensity values are approximately 10 times higher than the measurement. If one accepts the hypothesis that the absolute calibration was off by a factor of 10 for some reason for this particular set of experiments, then we can state that the present calculation reproduces the Marseille University data correctly.

C. Titan Conditions by the NASA Ames Group

Bose et al. [10] of NASA Ames Research Center performed an experiment to simulate Titan entry in a shock-tube facility using an N_2–CH_4 mixture. Measurement was made behind the primary shock wave. They obtained the calibrated intensity profiles for the CN violet and the CN red bands. Their experimental conditions were as follows:

1) Condition a used 2%CH_4–98%N_2 by volume, shock velocity $U_{sh} = 5.15$ km/s, and freestream pressure $p_\infty = 0.1$ torr.

2) Condition b used 5%CH_4–95%N_2, $U_{sh} = 5.56$ km/s, and $p_\infty = 0.1$ torr.

3) Condition c used 8.6%CH_4–91.4%N_2, $U_{sh} = 5.56$ km/s, and $p_\infty = 0.1$ torr.

4) Condition d used 8.6%CH_4–91.4%N_2, $U_{sh} = 5.93$ km/s, and $p_\infty = 1.0$ torr. The lateral depth of calculation was 10.16 cm.

The calculations made by Bose et al. [10] using the NEQAIR96 [2] code under the assumption of Boltzmann excitation at $p_\infty = 0.1$ torr for U_{sh} of 5.15 to 5.56 km/s did not agree with the experimental data. The difference was attributed by Bose et al. [10]to non-Boltzmann excitation. To explain the non-Boltzmann radiation, Bose et al. suggested a nonlocal collisional radiative model by taking the collisional excitation rates from the work of Zalogin et al. [32]. But this model still underpredicted the radiation intensities measured; especially, their model failed to predict the intensity decay rates.

Table 2 Determined values of C and D_a

	C	D_a, eV (K)[a]
Case a	100	7.63 (88,600)
Case b	100	6.88 (79,800)
Case c	100	5.95 (69,100)
Case d	1	$\leq$ 2.67 (31,000)

[a]Corresponding activation temperature D_a/k_B.

In the present numerical reconstruction of Bose et al's [10] case, the Landau–Teller model with $s = 1$ was used, as was done by Bose et al. Chemical-reaction models were taken from the reduced reaction set for N_2–CH_4–Ar mixtures summarized by Gökçen [31], as was done in the work of Bose et al. [10]. Intensity profiles of CN violet and CN red bands were computed for the four cases previously mentioned under both Boltzmann and non-Boltzmann excitations with and without radiative power loss. N, N_2, and electrons were considered as colliders in the QSS computation.

Figure 5 shows the results of flowfield and radiation calculation for case b. Because pressure in this test was lower than in either the KAIST or Marseille University tests, one expects a strong non-Boltzmann effect. First, radiative power loss of Q_r ($\zeta = 1$) was considered. In Fig. 5a, one sees that removal of vibroelectronic energy and total enthalpy by the radiative power loss pulls down the vibroelectronic and heavy-particle translational temperatures. The effect of non-Boltzmann excitation on temperatures is negligible. In Fig. 5b, the number densities of CH_2, CH_3, and CH_4 are not plotted because they are immediately dissociated behind the shock wave into the smaller species. Because of the radiative power loss, temperature decreases and the number density of CN increases slightly. Electron density decreases by about the factor of 3 toward the downstream.

As Fig. 5c shows, the populations of electronic states decrease substantially, presumably by the radiative power loss. One notes here, however, that the population of $A^2\Pi$ state does not decay as much as other states: the $A^2\Pi$ state is almost Boltzmann ($\kappa \sim 1$). But states $B^2\Sigma^+$, $a^2\Sigma^+$, and $D^2\Pi$ are substantially non-Boltzmann, with $\kappa = \sim 0.73$, 0.61, and 0.41 at $x = \sim 1$ cm. The corresponding radiation profiles for CN violet and CN red bands are presented in Fig. 5d. For CN violet, radiation intensity decays differently between the Boltzmann and non-Boltzmann cases; for CN red, that is not so. In any case, all calculations with Q_r ($\zeta = 1$) fail to predict the radiation profiles; the absolute intensity is overestimated and its decay rate is predicted to be substantially slower than the measurements. Though not shown, these trends also exist in cases a and c. Also note here that the slope of rise to the peak in the experiment is slightly smaller than calculated, which can again be attributed to the spatial smearing mentioned earlier.

To explain the disagreements mentioned previously, we first considered two possibilities: 1) shock attenuation effect and 2) deviation of electron-electronic temperature from vibrational temperature. The answer was negative: neither of these can explain the observed discrepancies. Boundary-layer thickness must be growing by a nonphysically large rate to explain the observed intensity decay rates. Even when electron-electronic temperature is taken to be different from the vibrational temperature (i.e., a three-temperature model [33,34] is used), all calculated quantities remain essentially the same.

Figures 6 and 7 present the radiation profiles of the CN violet and the CN red bands for cases a–d using the Landau–Teller model with a ζ value large than unity in Q_r', but using the excitation rate K_h. For CN violet, our calculations find the ζ value agreeing with experiment to be between 5 and 7 (i.e., about 6). At low pressure (cases a–c), the difference in radiation intensities under Boltzmann and non-Boltzmann excitations (when $\zeta = 6$) are small. The values of κ are about 1.0 and 0.72, respectively, for the $A^2\Pi$ and $B^2\Sigma^+$ states at around the peak radiation point. The intensity profiles of the calculated CN violet radiation almost keep track of the measured absolute intensities and their decay rates. But there is still a considerable discrepancy in the CN red band in its intensity decay rates. For the high-pressure case (case d), the falloff rates are very close to the measurements for CN violet. As Fig. 7d shows, the calculated absolute value of the CN red radiation overestimates by a factor of 4, as opposed to a factor of 10 in the Marseille University

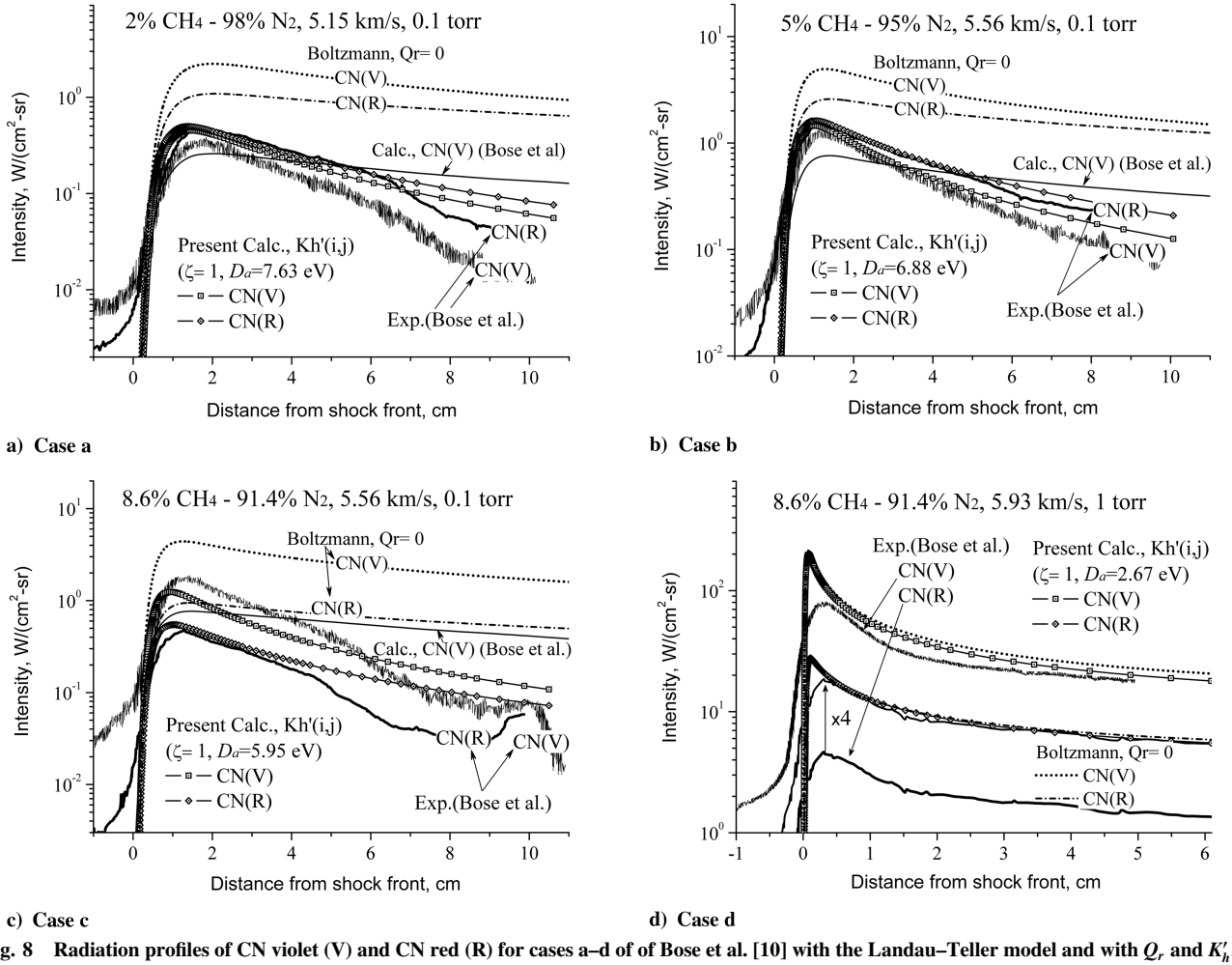

Fig. 8 Radiation profiles of CN violet (V) and CN red (R) for cases a–d of of Bose et al. [10] with the Landau–Teller model and with Q_r and K_h'.

data. In addition to the factor 4 discrepancy for the CN red, the present calculation with K_h underestimates the radiation decay rates for both the CN violet and CN red systems. When the bridging model is used, the time to rise to the peak intensity becomes slightly smaller.

Efforts have been made to explain the large radiation decay rates. Agreement was found only when the K_h was replaced by K'_h given in Eqs. (6) and (7). The parameters C and D_a used in generating K'_h are tabulated in Table 2. The results are shown in Fig. 8. As seen here, the radiation decay rates for both CN violet and CN red systems are numerically reproduced fairly well. The nonequilibrium factor κ varies from around 1.1 to 0.2 for the CN red and 0.5 to 0.1 for the CN violet in cases a–c. In case d, the κ varies from about 1.1 to 0.5 for both CN red and CN violet. The K'_h used implies a strong temperature dependence of the 1-to-2 transition rate in CN by heavy-particle collision, stronger than that corresponding to the energy gap between the two states, and a much smaller absolute rate, as shown in Fig. 1.

In Fig. 8, the present result is compared with the result of Bose et al. [10] on the radiation profile of CN violet. As seen in the figure, the present result agrees better with the experimental data.

IV. Discussion

The preceding results indicate that the newly developed SPRADIAN07 code package is accurate and better than the NEQAIR85 code package, at least when the internal distribution is Boltzmann, as in the experiment of the KAIST group. There may be two reasons for this: the radiation intensity parameters in the SPRADIAN07 package may be more accurate, and the more accurate handling of symmetries in the SPRADIAN07 code may be showing its effect.

In the intermediate-pressure range (i.e., in the pressure range of the Marseille University experiment), the SPRADIAN07 package seems to be able to at least partly reproduce the weakly non-Boltzmann distributions.

For the low-pressure, strongly non-Boltzmann, cases, even when using the K_h values of [7], the SPRADIAN07 package seems to give results that agree better with the experimental data than the NEQAIR96 package. But the K_h values of [7] fail to reproduce the slope of radiation decay at low pressures. Only when the K_h values are modified into K'_h do the calculations agree with the experimental data taken at such low pressures. As seen in Fig. 1, the cross sections implied by K'_h are quite reasonable. This means that the cross sections implied by K_h, which are 3 orders of magnitude larger than those implied by K'_h, are too large.

The cross sections used in deriving K_h values in [7] were taken from the experimental data on quenching of radiation mostly at room temperature. The procedure applied in [7] in determining K_h implicitly assumed a large excitation cross section near the threshold. As seen in Fig. 1, the K'_h implies that cross section rises gradually from zero at the threshold, which is quite reasonable. The present study indicates that the K_h values in [7] should be modified to account for this behavior before being applied to the non-Boltzmann cases.

V. Conclusions

The SPRADIAN07 code accurately reproduces the experimental data on CN radiation under a nonequilibrium condition taken in a shock tube when the pressure is relatively high and the internal distribution is Boltzmann, as in the experiment by the KAIST group. When pressure is intermediate and the internal distribution is weakly non-Boltzmann, as in the experiment by the Marseille University group, the existing SPRADIAN07 package can still reproduce most aspects of the measured CN radiation. When pressure is very low and the internal distribution is strongly non-Boltzmann, as in the experiment by the NASA Ames group, the SPRADIAN07 package with the existing data package on heavy-particle-impact excitation rates can reproduce some aspects of the experimental data, but not all. To numerically reproduce most aspects of the experimental data, radiative power loss by hitherto unknown band systems must be accounted for and the excitation rates must be lowered by 3 orders of magnitude. The existing excitation-rate-coefficient package in SPRADIAN07 must be modified.

References

[1] Park, C., "User's Manual: Nonequilibrium Air Radiation (NEQAIR) Program," NASA TM86707, July 1985.

[2] Whiting, E. E., Park, C., Liu, Y., Arnold, J. O., and Paterson, J. A., "NEQAIR96, Nonequilibrium and Equilibrium Radiative Transport and Spectra Program: User's Manual," NASA, Reference Publ. 1389, Dec. 1996.

[3] Fujita, K., and Abe, T., "SPRADIAN, Structured Package for Radiation Analysis: Theory and Application," Inst. of Space and Astronautical Science, Rept. 669, Tokyo, July 1997.

[4] Pfeiffer, B., Fertig, M., Winter, M., and Kurtz, M. A., "PARADE a Program to Calculate the Radiation of Atmospheric Re-Entry in Different Atmosphere," *Proceedings of the International Workshop on Radiation of High Temperature Gases in Atmospheric Entry*, ESA, Paris, 2003, pp. 85–91.

[5] Park, C., *Nonequilibrium Hypersonic Aerothermodynamics*, Wiley, New York, 1990.

[6] Park, C., "Rate Parameters for Electronic Excitation of Diatomic Molecules 1: Electron-Impact Process," AIAA Paper 2008-1206, 2008.

[7] Park, C., "Rate Parameters for Electronic Excitation of Diatomic Molecules 2: Heavy Particle-Impact Phenomenon," AIAA Paper 2008-1446, 2008.

[8] Lee, E. S., Park, C., and Chang, K. S., "Shock-Tube Determination of CN Formation Rate in a CO–N_2 Mixture," *Journal of Thermophysics and Heat Transfer*, Vol. 21, No. 1, Jan.–Mar. 2007, pp. 50–56. doi:10.2514/1.25144

[9] Rond, C., Boubert, P., Felio, J. M., and Chikhaoui, A., "Radiation Measurements in a Shock Tube for Titan Mixtures," *Journal of Thermophysics and Heat Transfer*, Vol. 21, No. 3, July–Sept. 2007, pp. 638–646. doi:10.2514/1.28422

[10] Bose, D., Wright, M. J., Bogdanoff, D. W., Raiche, G. A., and Allen, G. A., Jr., "Modeling and Experimental Assessment of CN Radiation Behind a Strong Shock Wave," *Journal of Thermophysics and Heat Transfer*, Vol. 20, No. 2, Apr.–June 2006, pp. 220–230. doi:10.2514/1.16869

[11] Park, C., "On Convergence of Computation of Chemically Reacting Flows," AIAA Paper 1985-247, June 1985.

[12] Park, C., "Assessment of Two-Temperature Kinetic Model for Ionizing Air," *Journal of Thermophysics and Heat Transfer*, Vol. 3, No. 3, July 1989, pp. 233–244. doi:10.2514/3.28771

[13] Vincenti, W. G., and Kruger, C. H., *Introduction to Physical Gas Dynamics*, Wiley, New York, 1965.

[14] Park, C., "Assessment of Two-Temperature Kinetic Model for Dissociating and Weakly-Ionizing Nitrogen," *Journal of Thermophysics and Heat Transfer*, Vol. 2, No. 1, Jan. 1988, pp. 8–16. doi:10.2514/3.55

[15] Millikan, R. C., and White, D. R., "Systematics of Vibrational Relaxation," *Journal of Chemical Physics*, Vol. 39, No. 12, 1963, pp. 3209–3213. doi:10.1063/1.1734182

[16] Sharma, S. P., Huo, W., and Park, C., "The Rate Parameters for Coupled Vibration-Dissociation Coupling in Generalized SSH Approximation," *Journal of Thermophysics and Heat Transfer*, Vol. 6, No. 1, Jan.–Mar. 1992, pp. 9–21. doi:10.2514/3.312

[17] Laux, C. O., "Optical Diagnostics and Radiative Emission of Air Plasmas," High Temperature Gasdynamics Lab., Stanford Univ., Rept. T-288, Stanford, CA, Aug. 1993.

[18] Bauschlicher, C. W., Langhoff, S. R., and Taylor, P. R., "Theoretical Study of the Dissociation Energy and the Red and Violet Band Systems of CN," *Astrophysical Journal*, Vol. 332, Sept. 1988, pp. 531–538. doi:10.1086/166675

[19] Kovács, I., *Rotational Structure in the Spectra of Diatomic Molecules*, Adam Hilger, London, 1969.

[20] Whiting, E. E., Paterson, J. A., Kovács, I., and Nicholls, R. W., "Computer Checking of Rotational Line Intensity Factors for Diatomic Transitions," *Journal of Molecular Spectroscopy*, Vol. 47, No. 1, July 1973, pp. 84–98. doi:10.1016/0022-2852(73)90078-7

[21] Levin, D. A., Candler, G. V., Collins, R. J., Erdman, P. W., Zipf, E. C., and Howlett, L. C., "Examination of Theory for Bow Shock Ultraviolet

Rocket Experiments 1," *Journal of Thermophysics and Heat Transfer*, Vol. 8, No. 3, 1994, pp. 447–452. doi:10.2514/3.563

[22] Levin, D. A., Braunstein, M., Candler, G. V., Collins, R. J., and Smith, G. P., "Examination of Theory for Bow Shock Ultraviolet Rocket Experiments 2," *Journal of Thermophysics and Heat Transfer*, Vol. 8, No. 3, 1994, pp. 453–459. doi:10.2514/3.564

[23] Park, C., "Spectral Line Intensities in a Nonequilibrium Nitrogen Plasma," *Journal of Quantitative Spectroscopy and Radiative Transfer*, Vol. 8, No. 10, Oct. 1968, pp. 1633–1653. doi:10.1016/0022-4073(68)90107-6

[24] Anon., "Cyano Radical: Constants of Diatomic Molecules," *NIST Standard Reference Database No. 69* [online database], http://webbook.nist.gov/chemistry [retrieved 27 Nov. 2007].

[25] Douglas, A. E., and Routly, P. M., "The Spectrum of the CN Molecule," *Astrophysical Journal Supplement Series*, Vol. 1, 1955, pp. 295–317. doi:10.1086/190010

[26] Lutz, B. L., "Spectrum of the CN Molecule 2: $F^2\Delta_r - A^2\Pi_i$," *Astrophysical Journal*, Vol. 164, Feb. 1971, pp. 213–216. doi:10.1086/150831

[27] Schaefer, H. F., III, and Heil, T. G., "Electronic Structures and Potential Curves for the Low-Lying States of the CN Radical*," *Journal of Chemical Physics*, Vol. 54, No. 6, 1971, pp. 2573–2580. doi:10.1063/1.1675214

[28] Herzberg, G., *Molecular Spectra and Molecular Structure I. Spectra of Diatomic Molecules*, Krieger, Malabar, FL, 1989.

[29] Huber, K. P., Klug, C. A., and Alberti, F., "Jet Emission Spectra in the Schumann Region: The $L^2\Sigma^- \rightarrow A^2\Pi_i$ Transition of CN," *Journal of Molecular Spectroscopy*, Vol. 124, No. 2, Aug. 1987, pp. 407–419. doi:10.1016/0022-2852(87)90150-0

[30] Lavendy, H., Gandara, G., and Robbe, J. M., "Oscillator Strengths, Radiative Lifetimes, and Photodissociation Cross-Sections for CN," *Journal of Molecular Spectroscopy*, Vol. 106, No. 2, Aug. 1984, pp. 395–410. doi:10.1016/0022-2852(84)90170-X

[31] Gökçen, T., "N_2–CH_4–Ar Chemical Kinetic Model for Simulations of Titan Atmospheric Entry," *Journal of Thermophysics and Heat Transfer*, Vol. 21, No. 1, Jan.–Mar. 2007, pp. 9–18. doi:10.2514/1.22095

[32] Zalogin, G. N., Kozlov, P. V., Kuznetsova, L. A., Losev, S. A., Makarov, V. N., Romanenko, Yu. V., and Surzhikov, S. T., "Radiation Excited by Shock Waves in a CO_2–N_2–Ar Mixture: Experiment and Theory," *Technical Physics*, Vol. 46, No. 6, 2001, pp. 654–661. doi:10.1134/1.1379629

[33] Lee, J. H., "Electron-Impact Vibrational Relaxation in High-Temperature Nitrogen," *Journal of Thermophysics and Heat Transfer*, Vol. 7, No. 3, 1993, pp. 399–405. doi:10.2514/3.432

[34] Mertens, J. D., "Computational Model of Nitrogen Vibrational Relaxation by Electron Collisions," *Journal of Thermophysics and Heat Transfer*, Vol. 13, No. 2, 1999, pp. 204–209. doi:10.2514/2.6437